

# Bubble counting using an inverse acoustic scattering method

Ramani Duraiswami,<sup>a)</sup> Sankar Prabhukumar, and Georges L. Chahine  
*Dynaflow, Inc., 7210 Pindell School Road Fulton, Maryland 20759*

(Received 19 February 1997; revised 30 April 1998; accepted 19 August 1998)

A nuclei size measurement technique is developed, based on a dispersion relation for propagation of sound waves through a bubbly liquid. This is used to relate the attenuation and phase velocity of a sound wave to the bubble population, leading to two integral equations. These equations are ill posed, and require special treatment for solution. Algorithms based on a minimization method that imposes a number of physical constraints on the solution, rendering the equation well posed, are developed. The procedure is first tested on analytical data with varying artificial noise added, and found to be successful in recovering the bubble density function, and to perform much better than other published solution techniques. Then, bubbles were generated using electrolysis and air injection through porous tubes, and bubble populations measured. Short monochromatic bursts of sound at different frequencies were emitted and received using hydrophones. The received signals were then processed and analyzed to obtain the attenuation and phase velocity. The void fraction and known experimental errors were also obtained and were fed as constraints to the inverse problem solution procedure. This resulted in bubble populations which compare favorably to those obtained by microphotography. © 1998 Acoustical Society of America. [S0001-4966(98)05811-1]

PACS numbers: 43.30.Es, 43.30.Pc, 43.20.Ye, 43.25.Yw [SAC-B]

## INTRODUCTION

Determination of the bubble population in a sample of liquid is an important problem in many fields. A significant amount of experimental work has been performed to determine the bubble size distribution in given samples of water (e.g., Refs. 1–11). These experiments can be divided into optical studies (including scattering, photographic, and holographic), acoustical studies (including scattering, attenuation, and dispersion), and others (including electrical impedance<sup>12</sup> and cavitation susceptibility<sup>13</sup>).

Acoustical methods are inverse methods, relying on the fact that bubbles have a strong effect on the propagation of acoustic waves. The acoustical cross section of a bubble is three to four orders of magnitude greater than its geometrical cross section.<sup>2</sup> Acoustical techniques are relatively simple, and applicable to much larger liquid samples. Additionally, the ocean is much more transparent to the passage of acoustic waves than it is to light.

The predictions of existing acoustical and optical techniques differ widely;<sup>14</sup> for instance, the acoustical method of Wildt<sup>15</sup> overpredicts the bubble population density by as much as two orders of magnitude at small radii, and underpredicts it significantly at larger radii. The error lies in the procedures used to infer the bubble population from the measurements. In this paper we present a consistent method for obtaining the bubble population from measurements.

Using a set of effective equations, derived by taking the limit of the complete equations of motion to small bubble volume fractions,<sup>16</sup> a dispersion relation for bubbly fluids was developed by Commander and Prosperetti.<sup>17</sup> This relationship was used to obtain the attenuation and phase velocity for *given bubble populations* and was compared very favorably with measurements. They also found that the

computed attenuation and phase velocity were quite sensitive to the bubble population distribution. Here, we use the inverse procedure and obtain two integral equations for the bubble population density in terms of the phase velocity and attenuation. Solution of these equations using *measured* values of the attenuation and change in phase velocity will allow computation of the bubble population. The problem faced in the solution of these equations is that the equations are ill posed. We considered in Refs. 18 and 19 several approaches for solving this ill-posed problem, and found that among the approaches tested one based on constrained minimization worked best.

In Sec. I we describe the governing equations of the problem and their characteristics. In Sec. II we present the details of our algorithm. In Sec. III we apply the algorithm to synthetic data obtained from assumed bubble populations and show that the algorithm is successful in recovering the bubble population. In Sec. IV, we describe experiments conducted to validate the method for measurement of the bubble population. The signal processing procedures used to analyze the signals are described in Sec. V. The method is applied to obtaining bubble populations from experiments in Sec. VI, and the resulting bubble populations validated against photographic data in Sec. VII. Conclusions are presented in Sec. VIII.

## I. GOVERNING EQUATIONS

Consider a bubbly medium consisting of a pure liquid of sound speed  $c_l$  containing spherical bubbles of different radii. The bubble size distribution in the liquid is characterized by the bubble population density,  $N(a)$ , defined such that

<sup>a)</sup>Electronic mail: ramani@dynaflow-inc.com

$$\int_{a_1}^{a_2} N(a) da = \text{number of bubbles with radii} \quad (1)$$

in  $[a_1, a_2]$  per unit volume.

Here  $a$  denotes the equilibrium radius of the bubbles.  $N$  thus is a density and has SI units: number/m<sup>-4</sup>.

When sound of frequency  $\omega$  propagates through the bubbly medium, the bubbles oscillate, and extract and reradiate energy into the medium, thereby making it dispersive. Each bubble may be treated as an oscillator with a characteristic natural frequency  $\omega_0$  and a damping constant  $b$  that depend upon the frequency of the insonifying wave and the radius of the bubble. The effect of this dispersive behavior is to make the sound speed in the mixture,  $C_m$ , complex.

A dispersion relation relating the complex sound speed in the mixture to the sound speed in the pure medium, as a function of the bubble density function, was derived by Commander and Prosperetti,<sup>17</sup> on the basis of effective equations for sound propagation in bubbly liquids (valid at low bubble void fractions) obtained by Caffisch *et al.*<sup>16</sup> This equation is the starting point of our work, and is

$$\frac{c_l^2}{C_m^2} = 1 + 4\pi c_l^2 \int_{a_{lo}}^{a_{hi}} \frac{aN(a)}{\omega_0^2 - \omega^2 + 2ib\omega} da, \quad (2)$$

where  $i$  represents the imaginary unit.

Equation (2) enables computation of the complex speed of sound in the bubbly mixture,  $C_m$ , for a monochromatic wave of frequency  $\omega/2\pi$  for known bubble population distribution and known bubble natural frequencies and damping. We use the expressions obtained in Ref. 20 for the bubble natural frequency and the damping. These are obtained on the basis of a linearized study of the oscillation of a single gas bubble in response to a monochromatic wave, and are

$$\omega_0^2 = \frac{p_\infty - p_v + 2\sigma/a}{\rho a^2} \left( \Re(\Phi) - \frac{2\sigma}{ap_0} \right), \quad (3)$$

$$b = \frac{2\mu}{\rho a^2} + \frac{p_0}{2\rho a^2} \Im(\Phi) + \frac{\omega^2 a}{2c} = b_v + b_{th} + b_{ac}. \quad (4)$$

Here,  $p_\infty$  refers to the liquid equilibrium pressure,  $p_v$  the liquid vapor pressure in the bubble,  $\sigma$  is the surface tension, and the quantity  $p_0$  is the gas pressure in the bubble at equilibrium and is given by

$$p_0 = p_{g0} + p_v = p_\infty + \frac{2\sigma}{a}. \quad (5)$$

Here  $p_{g0}$  is the pressure due to noncondensable gases in the bubble;  $\Re$  and  $\Im$ , respectively, refer to the functions that yield the real and imaginary parts of a complex quantity. The three parts making up the expression for  $b$  are the damping due to viscosity, thermal effects, and acoustic reradiation. The quantity  $\Phi$  is given by

$$\Phi = \frac{3\gamma}{1 - 3(\gamma - 1)i\chi[(i/\chi)^{1/2} \coth(i/\chi)^{1/2} - 1]}, \quad (6)$$

where  $\gamma$  is the ratio of specific heats for the gas in the bubble, and where

$$\chi = \frac{D}{\omega a^2}, \quad (7)$$

with  $D$  the gas thermal diffusivity.

The dispersion relation (2) can be separated into its real and imaginary parts to obtain two new equations for  $N(a)$ , as

$$\frac{c_l}{C_M} = u - iv. \quad (8)$$

Doing so, one obtains

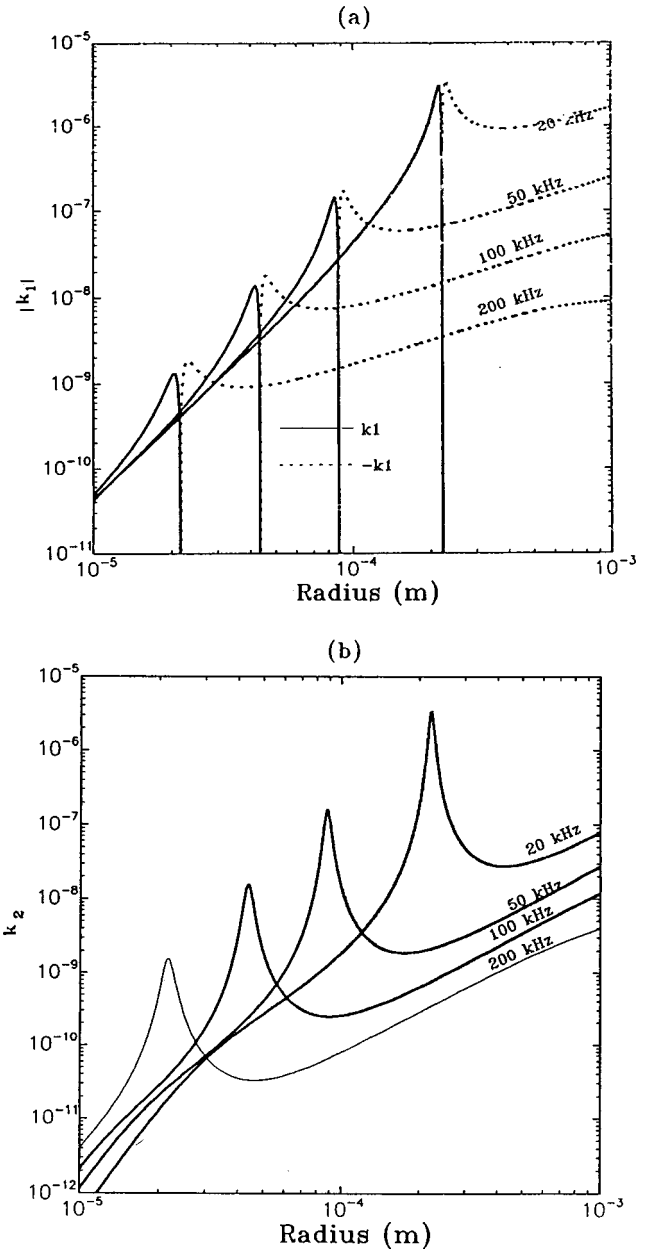


FIG. 1. The kernel functions  $|k_1|$  and  $k_2$  are plotted against the bubble radius for different insonification frequencies. The function  $k_2$  is peaked at the radius corresponding to resonance at the insonification frequency, but has a strongly growing tail which can be of the same order of magnitude as the peak. Since the function  $k_1$  is zero at the resonant radius and negative for larger radii these values are shown with a dotted line.

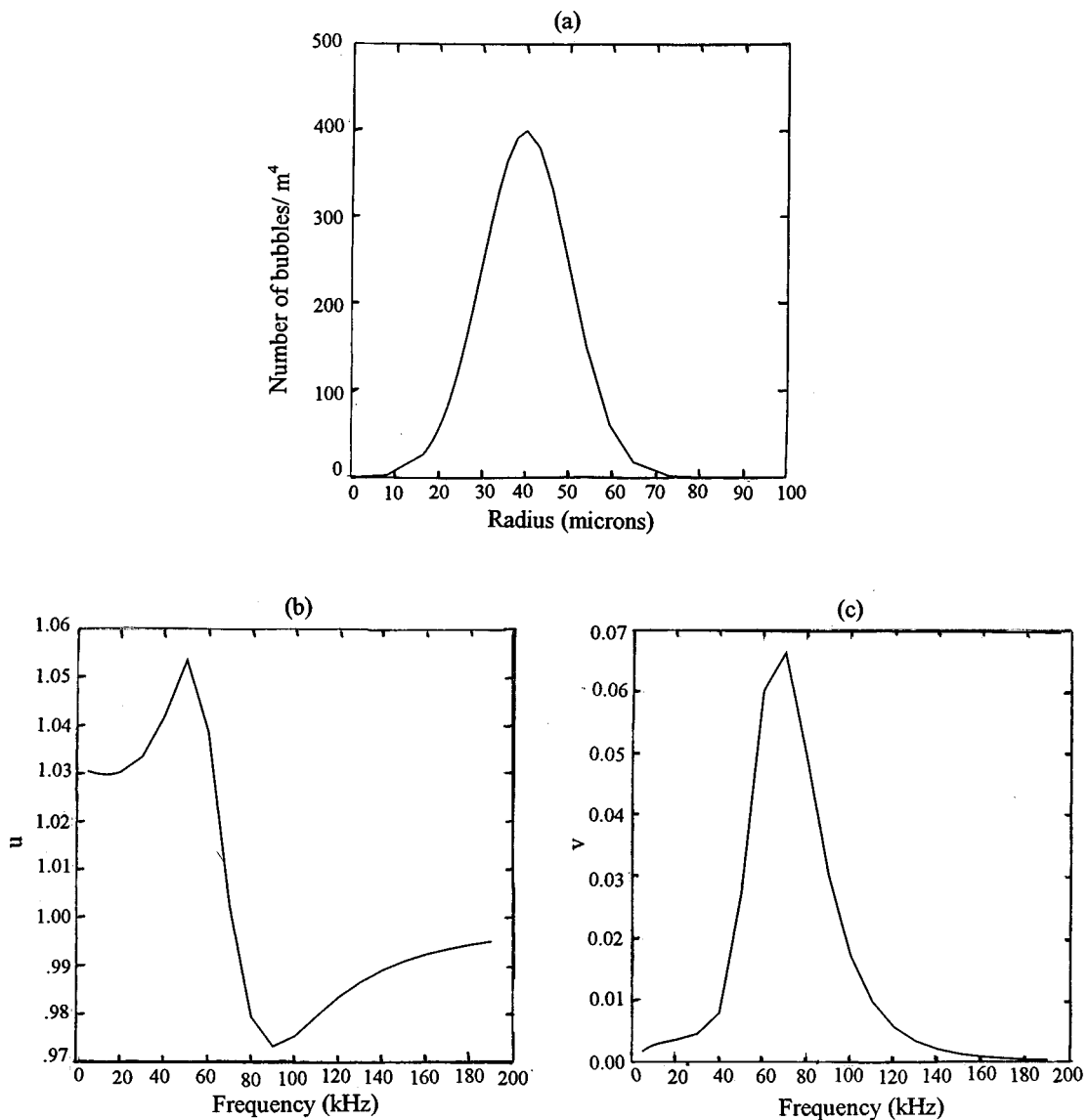


FIG. 2. (a) Assumed bubble density function, (b) corresponding  $u$  and (c) corresponding  $v$  curves produced by using the dispersion relation.

$$4\pi c_l^2 \int_{a_{lo}}^{a_{hi}} \left[ \frac{(\omega_0^2 - \omega^2)a}{(\omega_0^2 - \omega^2)^2 + 4b^2\omega^2} \right] N(a) da$$

$$= \int_{a_{lo}}^{a_{hi}} k_1(a, \omega) N(a) da = u^2 - v^2 - 1, \quad (9)$$

$$4\pi c_l^2 \int_{a_{lo}}^{a_{hi}} \left[ \frac{b\omega a}{(\omega_0^2 - \omega^2)^2 + 4b^2\omega^2} \right] N(a) da$$

$$= \int_{a_{lo}}^{a_{hi}} k_2(a, \omega) N(a) da = uv, \quad (10)$$

where we have introduced the notation  $k_1$  and  $k_2$  to denote the kernels of the two integral equations. These kernels are the crucial input of this model to the computations. These in turn depend upon accurate evaluation of the bubble resonance frequency,  $\omega_0$ , and the damping,  $b$ . As a check on the procedure for evaluating the resonance frequency and the damping we have reproduced all the results presented for them in Ref. 20. Figure 1 shows the two kernel functions.

The quantities  $u$  and  $v$  may be obtained by measuring the phase velocity  $c_m$  and the attenuation  $A$  of the wave in the bubbly liquid. We note that for a wave propagating with the mixture speed  $C_M$ , quantities are proportional to

$$\exp i\omega \left( t - \frac{x}{C_M} \right) = \exp i\omega \left( t - \frac{x}{c_l} (u - iv) \right)$$

$$= \exp \left( - \frac{\omega v x}{c_l} \right) \exp i\omega \left( t - \frac{x}{c_l/u} \right). \quad (11)$$

The phase velocity  $c_m$  of the sound wave is given by

$$c_m = c_l/u, \quad (12)$$

while the attenuation  $A$ , in dB per unit length, is given by

$$A = 20 \log_{10} e \left( \frac{\omega v}{c_l} \right), \quad (13)$$

where  $e = 2.71828$  is the base of the natural logarithms.

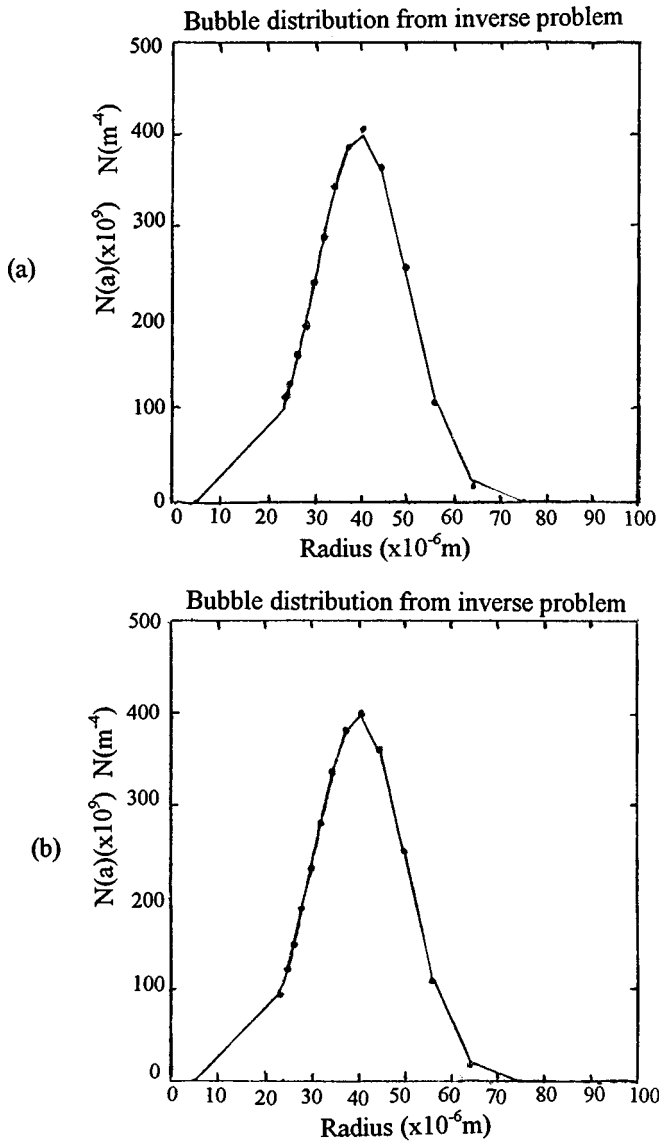


FIG. 3. Inverse problem solution for the bubble density  $N(a)$  using the non-negativity and noninfinity constraints and (a)  $K_1$  terms alone as objective functions and (b)  $K_2$  terms alone as objective functions.

In our experiments, where we emit short bursts of monochromatic waves. These quantities are calculated as follows:

$$u(f) = \frac{c_l \Delta t}{d_{ER}}, \quad v(f) = -\frac{c_l \log[\bar{p}^2(f)/\bar{p}_{ref}^2(f)]}{4\pi f d_{ER}}, \quad (14)$$

where

$$\bar{p}^2(f) = \frac{1}{T} \int_0^T p^2 dt, \quad (15)$$

where  $p(t)$  is the raw pressure signal at the measurement location. This quantity is referred to as the mean square amplitude (MSA) of the pressure signal. The other quantities are described below:

$f = \omega/2\pi$	frequency of the insonifying wave
$d_{ER}$	distance between emitter and receiver
$c_l$	speed of sound in the pure liquid (water)
$\Delta t$	time for signal to travel between hydrophones

$\bar{p}_{ref}^2(f)$  MSA of the pressure signal at a distance  $d_{ER}$  in pure water

$\bar{p}^2(f)$  MSA of a pressure signal at a distance  $d_{ER}$  in the bubbly medium

### A. Comments on the equations

Integral equations relating the bubble population to attenuation, or to backscattering, were presented in Ref. 15 in 1945, and have been used by several investigators. Sarkar and Prosperetti<sup>21</sup> showed that the earlier equations can be obtained from the dispersion relation (2) by making a binomial expansion valid at low void fraction. In this case the phase velocity can be taken to be that in the pure liquid, and the integral equation with  $k_1$  kernel becomes of higher order, while that with the  $k_2$  kernel survives. The present equations thus must be considered to hold at higher void fractions than these earlier equations.

It should be noted that the present procedure for obtaining the bubble density *requires* simultaneous knowledge of the attenuation and phase velocity. However, if these are known, each equation, (9) or (10), can be used independently to solve for the bubble population. In the method developed below we find a population that satisfies best both equations simultaneously.

It is useful to restate the assumptions inherent in these equations before designing an experiment that uses them. The theory of Caffisch *et al.*<sup>16</sup> is valid at low void fraction, and the bubbles are assumed to oscillate spherically. The analysis used to obtain the natural frequencies and attenuation also assumes spherical oscillations, with small deviations of the bubble instantaneous radius from the mean value. This requires that the pressure fields experienced by the bubbles be of small amplitude. Further, the bubbles are assumed to oscillate in a linear fashion (without exciting subharmonics or higher harmonics). The derivation of the expression for  $\Phi$  also requires the insonifying waves to be monochromatic. Thus in the experiments, we must make sure that these criteria are satisfied.

## II. INVERSE PROBLEM SOLUTION

Equations (9) and (10) obtained for the bubble distribution are *Fredholm integral equations* of the first kind (IFK) with analytic, compact kernels, and are consequently ill posed.<sup>22</sup> The ill posedness exhibits itself by making solutions to the equations discontinuous with respect to the problem data. Continuity of the solution of a mathematical model with respect to data is important for practical reasons, since experiments are prone to measurement errors and numerical computations are subject to round-off and other errors. For an ill-posed problem this may result in the error in the solution oscillating wildly when refining discretization until finally the "solution" has little relation to the original data. It is then necessary to look for the solution of a stable approximate problem, which in some sense is the closest to the exact solution, and is achieved by constraining the possible solutions of the problem. This process is termed *regularizing* the problem.

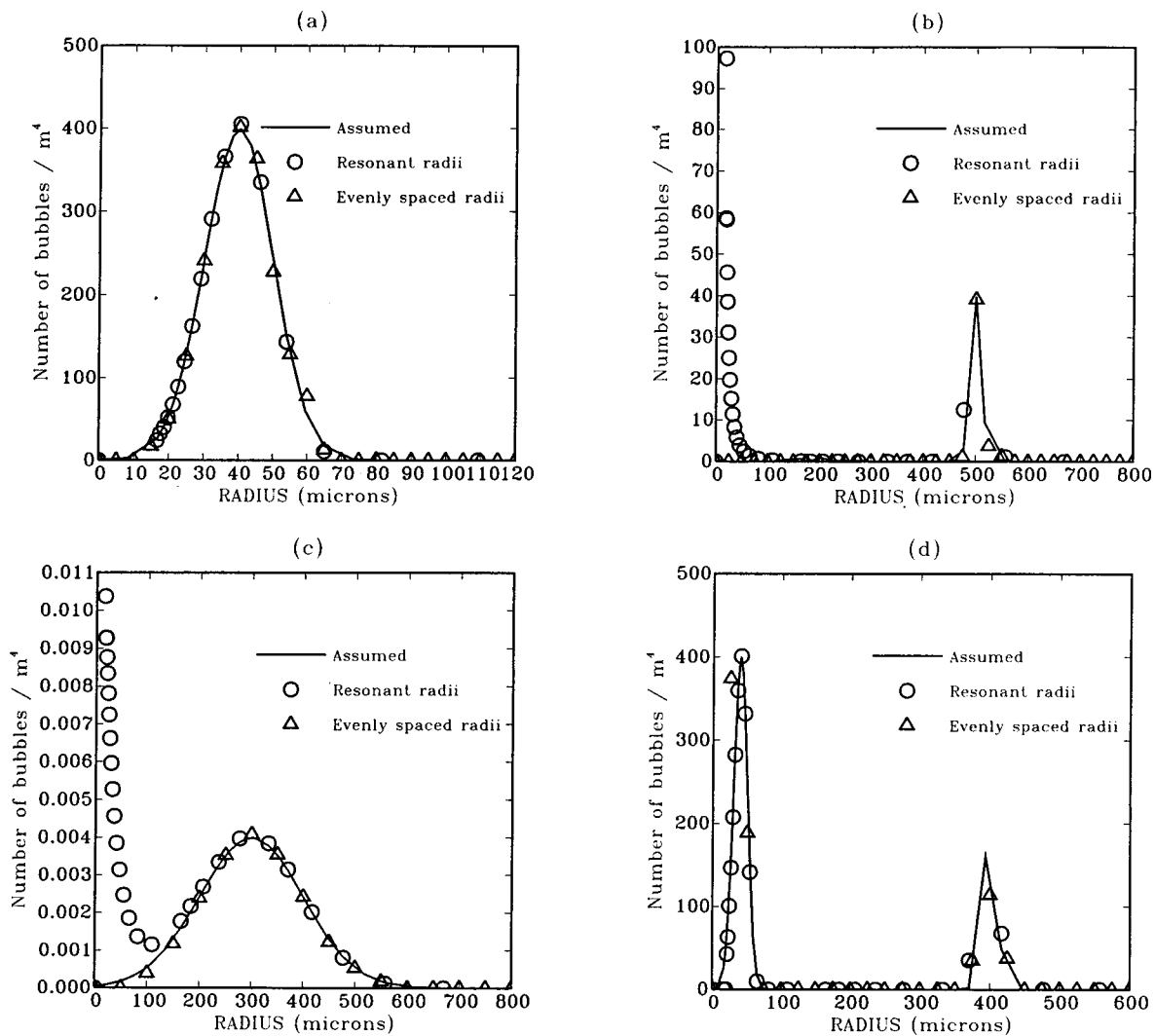


FIG. 4. Inverse problem solution checkout on four assumed bubble distributions using two methods of distributing collocation points: radii based on the peaks of  $k_2$ , and evenly spaced radii. (a) Single peak distribution with the peak at  $40 \mu\text{m}$  and standard deviation =  $10 \mu\text{m}$ . (b) Single peak distribution with the peak at  $500 \mu\text{m}$  and standard deviation =  $10 \mu\text{m}$ . (c) Single peak distribution with the peak at  $300 \mu\text{m}$  and standard deviation =  $100 \mu\text{m}$ . (d) Double peak distribution with peaks at  $40$  and  $400 \mu\text{m}$  and standard deviation =  $10 \mu\text{m}$  for both peaks. The method based on evenly spaced radii is able to capture the correct solution in all cases. Twenty-eight frequencies between  $5$  and  $190 \text{ kHz}$  were used for interrogation.

### A. Constraints on the bubble density function

An ill-posed problem can be regularized by imposing *a priori* constraints on the solution. Imposition of these constraints explicitly restricts the solution set, and can restore uniqueness and/or well posedness to the solution. Two techniques for accomplishing this task have been suggested in Ref. 23. These are based on the concepts of “prior knowledge” and “parsimony.” The first requires that all prior physical knowledge about the solution be included in the modeling, while the second requires that of all solutions not eliminated by the first principle, the one that adds the least amount of “new information,” be selected. The second condition prevents the introduction of nonphysical phenomena, which are artifacts of the solution technique.

For the bubble-counting problem the following information about the expected solution is known:

- (1) The function  $N(a)$  is strictly positive or equal to zero.
- (2) The function is expected to be a piecewise smooth continuous function of  $a$ .

- (3) The limits of integration, and discretization, for the radius can be set to some expected minimum and maximum radius, say  $a_{lo}$ ,  $a_{hi}$ .
- (4) The solution should depend continuously on the data, e.g., small changes in the measured attenuation should be associated with small changes in the bubble density.
- (5) The distributions obtained from the solution of one of the equations (9) and (10) should satisfy the other equation.
- (6) The volume fraction and surface area per unit volume of bubbles is bounded.

While these conditions might seem “obvious,” in the case of an ill-posed problem *a priori* imposition of such conditions during the solution process is essential to restore well posedness.

### B. Discretization of the integral equation

Numerical solution of the integral equations involves discretization, interpolation of the unknown function  $N(a)$

using a parametric interpolant, numerical quadrature to perform the integrals, and solution of the systems of linear equations and inequality constraints thus obtained. The method we found to be most robust for the present problem<sup>17</sup> was to divide the range over which the integral was done,  $[a_{lo}, a_{hi}]$  into  $M$  subdomains, with the unknown function interpolated linearly as follows:

$$N(a) = N_i \frac{a - a_{i+1}}{a_i - a_{i+1}} + N_{i+1} \frac{a - a_i}{a_{i+1} - a_i} \\ = N_i A(a) + N_{i+1} B(a), \quad (16)$$

where  $A(a)$  and  $B(a)$  represent the linear spline basis functions. The discretized equations then are

$$\sum_{i=1}^M \left[ \int_{a_i}^{a_{i+1}} k(\omega, a) A(a) da + \int_{a_{i-1}}^{a_i} k(\omega, a) B(a) da \right] N \\ = \alpha(\omega).$$

The integrations over the subdomains are performed using a 12-point Gauss-Legendre scheme. The equations are then written in linear system form by using collocation at the breakpoints between the subdomains. The data obtained at each frequency  $\omega_j$  results in a new equation, and these equations can be combined in a standard linear system as

$$KN = \alpha. \quad (17)$$

In all our computations we scale the matrices and the intervals of integration by the corresponding leading term to ensure that  $O(1)$  quantities are dealt with throughout.

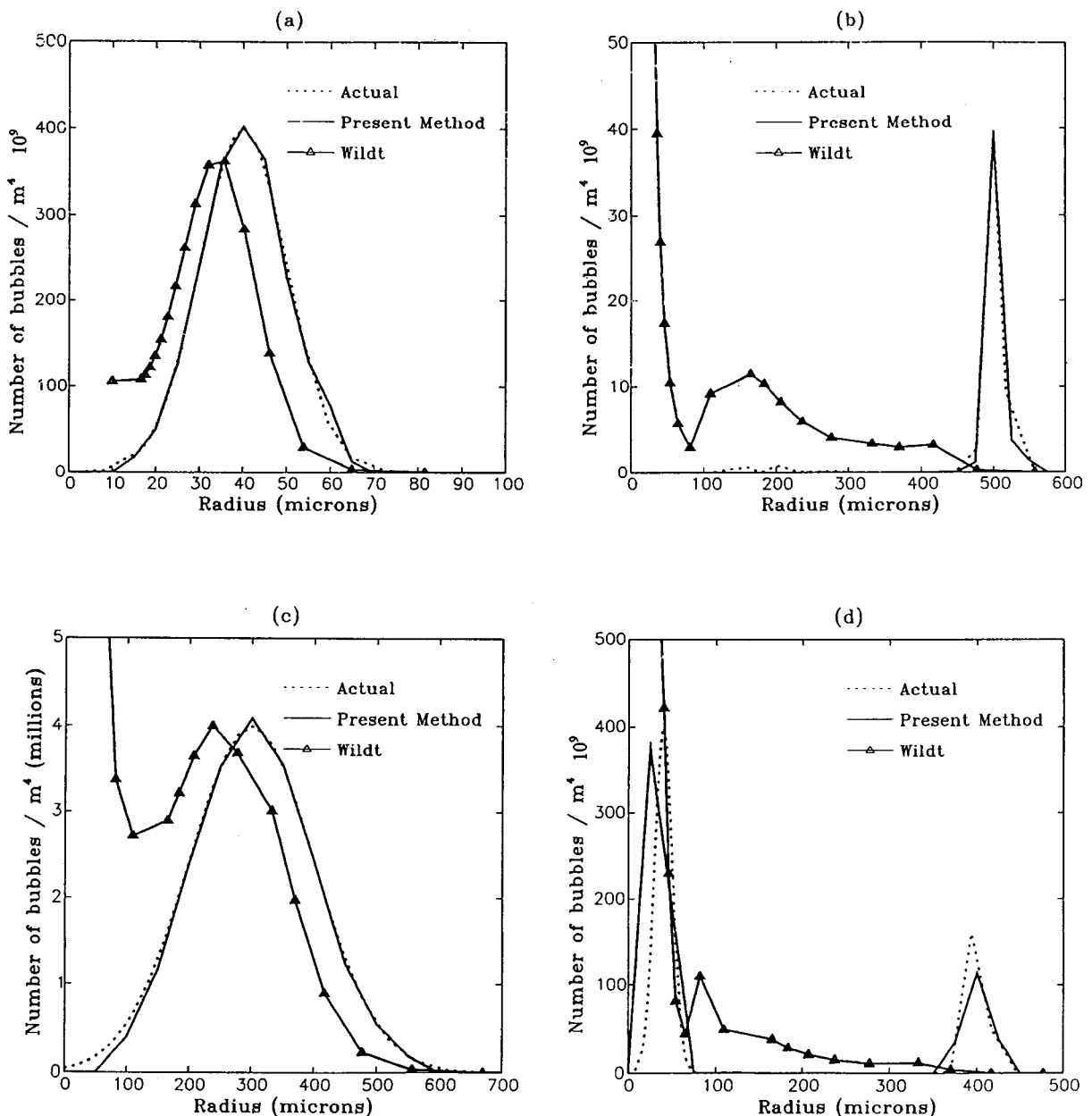


FIG. 5. Comparison of the present technique with the Wildt technique for four assumed bubble distributions.

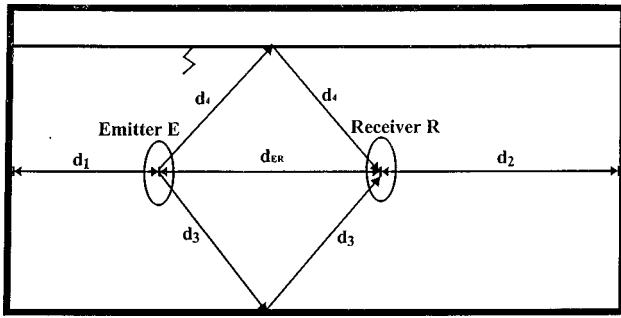


FIG. 6. Sketch of signal paths in a finite size tank.

### C. Solution via constrained minimization

Several techniques for achieving well-posed solutions to the inverse problem were considered in Ref. 18. Of these, the following method based on linear optimization was found to be most successful.

The motivation for using this technique was that classical techniques such as the Tikhonov regularization method<sup>22,24</sup> do not allow imposition of all available physical constraints. Rather, they only impose some mathematical constraints such as smoothness or bound on the norm of the solution. Here, since we have two sets of equations for the bubble population (9) and (10), in the Tikhonov method the equations have to be solved separately, and the error in the residue of the second equation can only be checked *a posteriori*.

The methods used in the field of *constrained optimization* seem particularly appropriate for this problem. In Refs. 18 and 19 we cast the integral equations as a linear optimization problem by using a simplex method.<sup>25</sup> This method seems very useful for the present problem because

- (1) The solution is guaranteed to be positive, without having to impose non-negativity as an explicit constraint.
- (2) Upon solution, constraint errors are immediately available.
- (3) The solution is minimized in the  $L_1$  norm.
- (4) Imposition of additional constraints does not require reformulation of the problem.
- (5) Additional regularization techniques such as Tikhonov regularization, which provide further linear equations, can be easily introduced in the framework.

In this approach our objective function for minimization is  $|K_2N - \alpha_2|$ , subject to the constraints

$$K_1N = \alpha_1, \quad N(a) \geq 0, \quad (18)$$

$$\int_{a_{10}}^{a_{hi}} N(a)a^2 da < C_1, \quad \int_{a_{10}}^{a_{hi}} N(a)a^3 da < C_2.$$

Here, the objective function comes from Eq. (10), and the first constraint comes from the fact that Eqs. (9) and (10) must be simultaneously satisfied. Also,  $C_1$  and  $C_2$  are constants which are larger than the expected surface area per unit volume and the volume fraction of bubbles. If information about these parameters is not available, they can be set to very large numbers. Incorporation of further experimental

### ABS ANALYSIS PROCEDURE

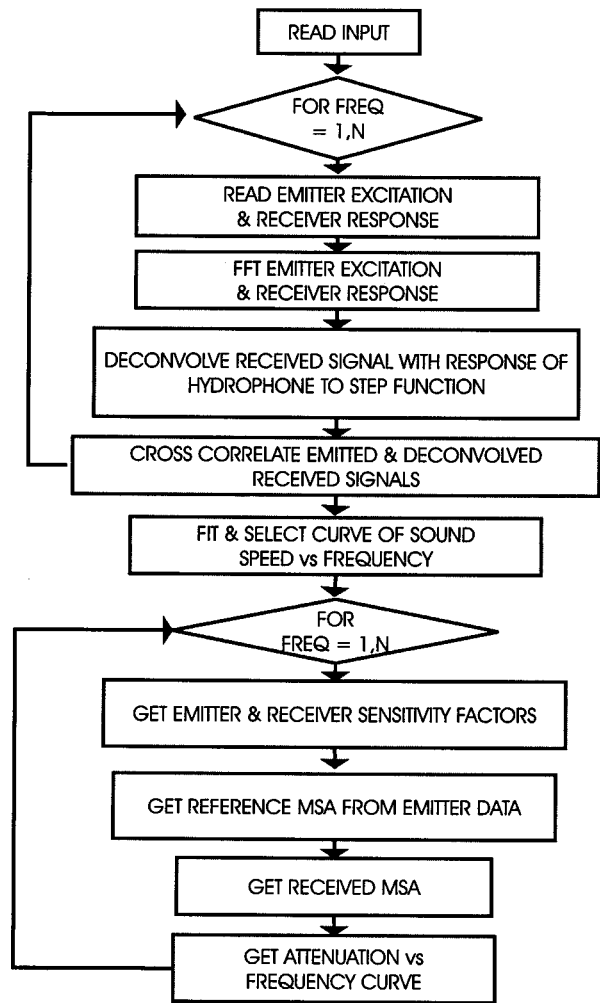


FIG. 7. Signal analysis procedure used in the acoustic bubble spectrometer (ABS).

constraint information in the solution procedure can be made.

If the data is available for  $M$  frequencies, we usually compute the matrices on the right-hand side at up to  $1.5M$  different radii, to reduce the quadrature errors in the representation of the  $K_{ij}$ . The use of the constrained optimization formulation lets us accurately calculate the bubble density function at more points than insonification frequencies.

### III. ANALYSIS OF THE SOLUTION PROCEDURE

Direct solution of an ill-posed inverse problem can give large errors if the input data contains small errors. The accuracy of a regularization scheme will depend upon the constraints used in the procedure, as well as numerical errors in the solution. In the following we performed a series of calculations to study the effect of these constraints on the accuracy of the obtained bubble distribution by using synthetic input data corresponding to a known bubble distribution. Input dispersion  $u$  and  $v$  data were generated using a given bubble distribution and the inverse problem solved using this data. This data was also used with the conventional method

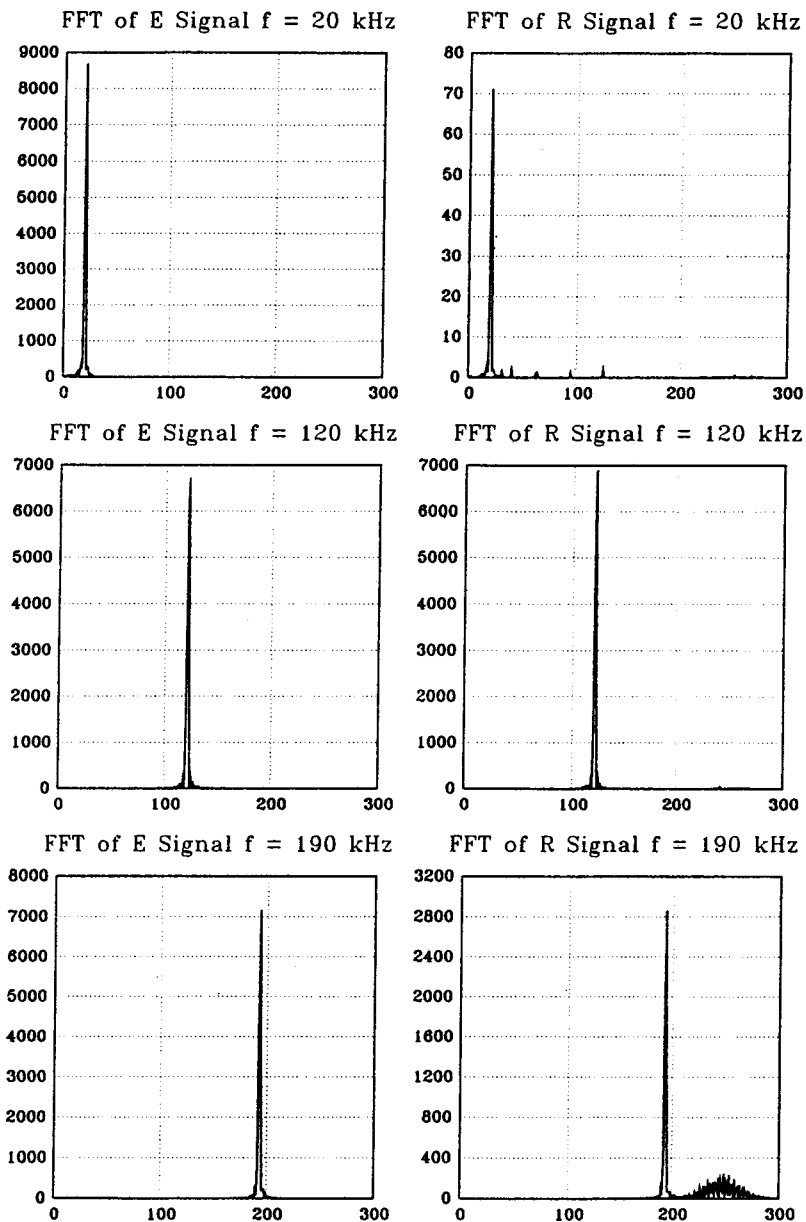


FIG. 8. Example emitter excitation and receiver response signals at three frequencies recorded during experiments performed with bubbles being generated using electrolysis with stainless steel wires of diameter 0.4 mm. Amplitude scale is arbitrary.

of solving the bubble counting problem, and a systematic comparison performed.

### A. Effect of imposing different constraints on the solution

A bubble distribution was assumed, and used with the dispersion relation to obtain corresponding  $u$  and  $v$  curves. Figure 2(a) shows the distribution and Fig. 2(b) and (c) shows the corresponding  $u$  and  $v$  curves.

Figure 3(a) and (b) shows the results of solving the problem using equations corresponding to either  $K_1$  and  $K_2$  as objective functions separately and imposing the non-negativity of  $N(a)$  and noninfinity constraints on the void fraction and surface area free unit volume. The figure shows that in this case the inverse problem solution procedure is able to obtain the assumed solution with either of the kernels  $K_1$  or  $K_2$ .

However, on some data with input errors of the order of

1%, we found that use of the  $K_1$  equations resulted in impossibility of satisfaction of the system of equations and constraints. For such problems we substantially relax the  $K_1$  constraints and effectively only use the equations involving  $K_2$  and the remaining constraints.

### B. Effect of the selection of the collocation points

The accuracy of the inverse problem solution depends upon the accuracy of the discretization—since the kernel functions at a particular frequency of insonification have peaks near the resonant radius corresponding to that frequency (see Fig. 1). More points near that radius are needed to adequately resolve the integral. Resonant radii not being the same for different frequencies one would need very many points for adequate resolution of the integral for all kernels. Thus there is a tradeoff in choosing more points to resolve the integral and ending up with too large and unstable a

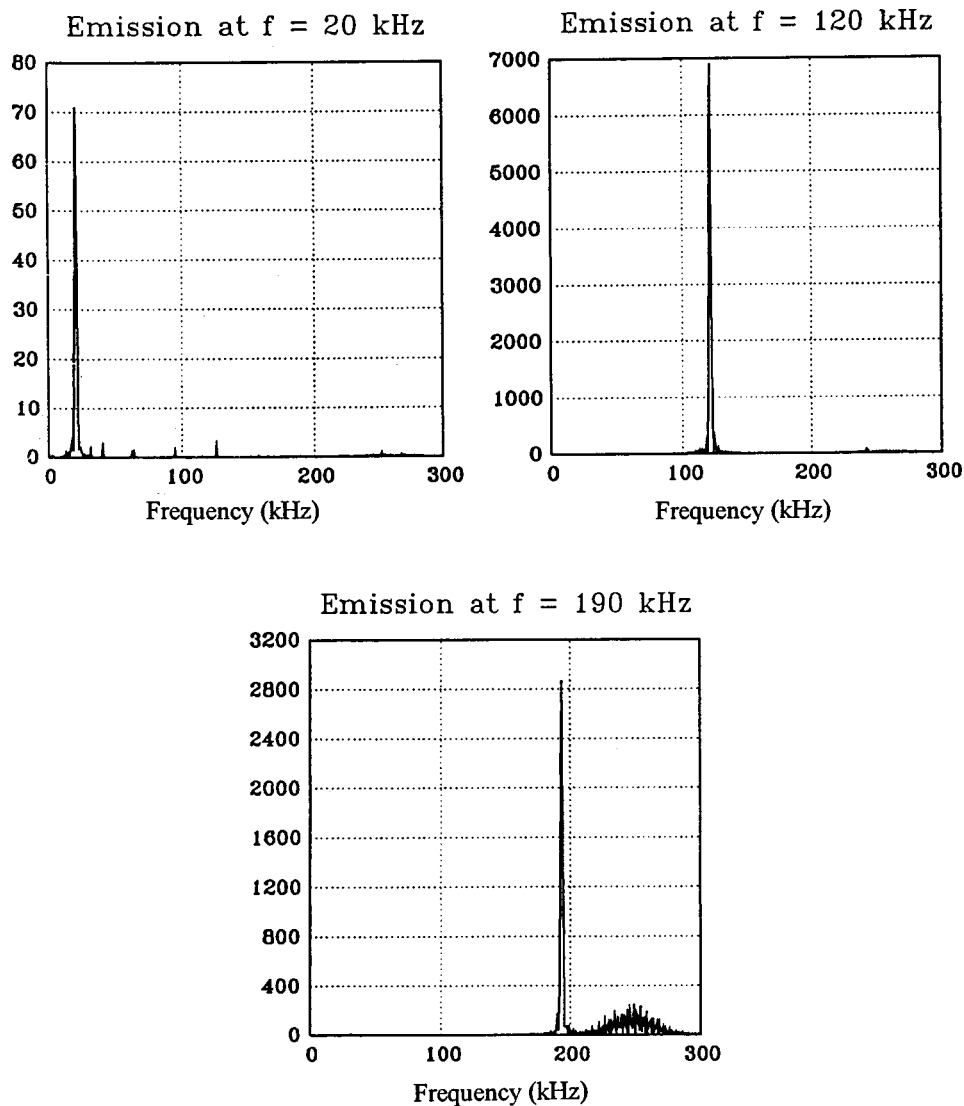


FIG. 9. Example fast Fourier transform results for received signals at three typical frequencies with generation of bubbles by electrolysis. Note that the signal remains monochromatic despite the presence of bubbles and indicates that we are operating in the linear acoustic regime of theory. Amplitude scale is arbitrary.

linear system. To decide on an optimal strategy the solution quality was studied on three sample bubble populations, constructed from an exponential distribution:

**A.** a single peak distribution with the peak at  $40 \mu\text{m}$ , and a standard deviation of  $10 \mu\text{m}$ ,

**B.** a single peak distribution with the peak at  $500 \mu\text{m}$ , and a standard deviation of  $10 \mu\text{m}$ ,

**C.** a single peak distribution with the peak at  $300 \mu\text{m}$ , and a standard deviation of  $100 \mu\text{m}$ , and

**D.** a bimodal distribution with one peak at  $40 \mu\text{m}$  and the other at  $400 \mu\text{m}$ , with a standard deviation of  $10 \mu\text{m}$  for each peak.

The inverse problem in each case was solved using two different ways to choose the discretization radii:

- (1) using the radii corresponding to the peaks of the kernel  $k_2(a, \omega_i)$  curve at each insonification frequency,  $\omega_i$ , and
- (2) using radii evenly distributed in the range  $(a_{lo}, a_{hi})$ .

Figure 4 shows the results obtained on solving the inverse problem using the two methods. On distributions A

and D both methods achieved satisfactory reconstructions. However, on distributions B and C the method with evenly spaced radii was remarkably better. We suspect this is due to the fact that the collocation points become very far apart in the region of large radii, unless the frequencies of insonification are chosen to be very close to each other (fractions of a kilohertz), and consequently the integrals cannot be resolved accurately. Through the matrix formulation this error is propagated to all radii and causes the whole method to become inaccurate.

Based upon these results we chose distributions of radii that were relatively even, and with the insonification frequencies that yield resonant radii corresponding to the collocation points, subject to a minimum separation in frequencies of 1 kHz.

### C. Comparison of the results of the present method with previous solution methods

The present results were compared with the solution procedure of Wildt.<sup>15,26</sup> In this approach a low volume frac-

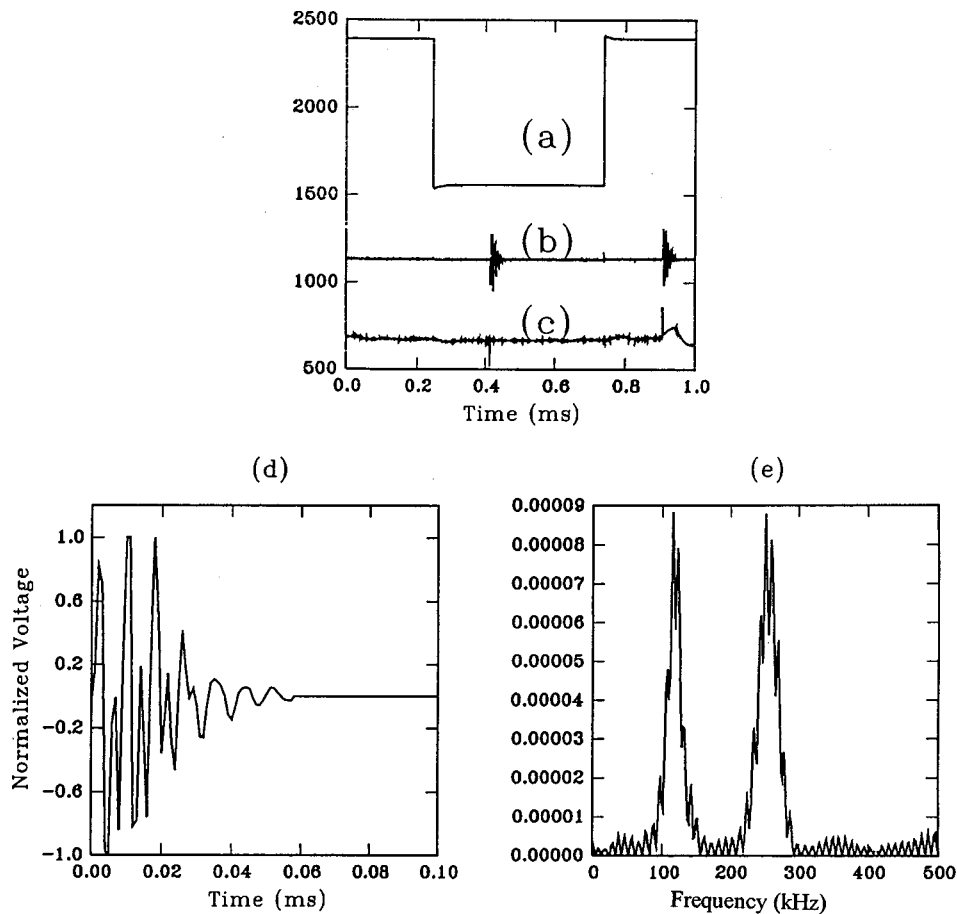


FIG. 10. (a) Input square wave used to excite the emitting hydrophone. (b) Signal received in response to the square wave. (c) Signal deconvolved with the response to a square wave of the system to a square wave. (d) Response function of emitter-receiver hydrophone system [a blow up of (b)]. (e) The FFT of the response to a square wave. Amplitude scale is arbitrary.

tion argument is used to set  $u$  to unity, and only the integral equation with kernel  $k_2$  is considered. This equation is solved by using the argument that the primary contribution to the integral arises from bubbles that are close to the frequency of insonification, and allows replacement of many components in the kernel by their values at resonance.<sup>21</sup> The final formula obtained for the bubble size distribution  $N(a)$  is

$$N(a_R) = \frac{4f^2 v}{c_l^2 a_R^2}, \quad (19)$$

where  $a_R$  is the resonant radius corresponding to the insonification frequency,  $f$ . Thus this formula predicts a bubble population that is essentially a scaled version of the attenuation curve. This formula has been used by several researchers over the last five decades.<sup>1-6,8</sup> Deficiencies in its ability to capture the solution were pointed out in Ref. 26.

The solutions obtained by this method and by the method developed were compared for the four bubble population distributions of Fig. 4. Figure 5(a)–(d) shows that for case (a) the Wildt method show bubble distributions that follow the general trend of the assumed curve, and produce bubble populations which have the same order of magnitude. However, for the other three distributions a wide departure from the assumed solution is seen especially for very small radii where the predicted populations are several orders of

magnitude higher. In each case the present constrained optimization solution is able to capture the correct solution.

The variance of the results of these methods from the current one can be explained by observing the nature of the kernel function  $k_2$  (see Fig. 1). At a given frequency this function is characterized by a sharp peak at the resonant radius with decay in each direction away from the radius. However, at larger radii the function grows, and the “tail” of the function corresponding to these larger radii approaches the values at the peak. Comparing the functions corresponding to different frequencies of insonification we see that the magnitude of the function for larger frequencies is much smaller than that for smaller frequencies. In the conventional methods the attenuation in the signal at the higher frequency is wrongly attributed to small bubbles. Further, many more small bubbles are needed to achieve the same attenuation in the signal. The cumulative result of the presence of bubbles of several sizes is the overestimation of bubbles of smaller sizes. We speculate that the widespread adoption of power law profiles for bubble population densities can, at least in part, be attributed to this feature of the solution, as has also been noted in Refs. 14 and 26.

#### IV. EXPERIMENTAL SETUP

The basic experimental procedure consists of emitting signals of various frequencies using a hydrophone located in

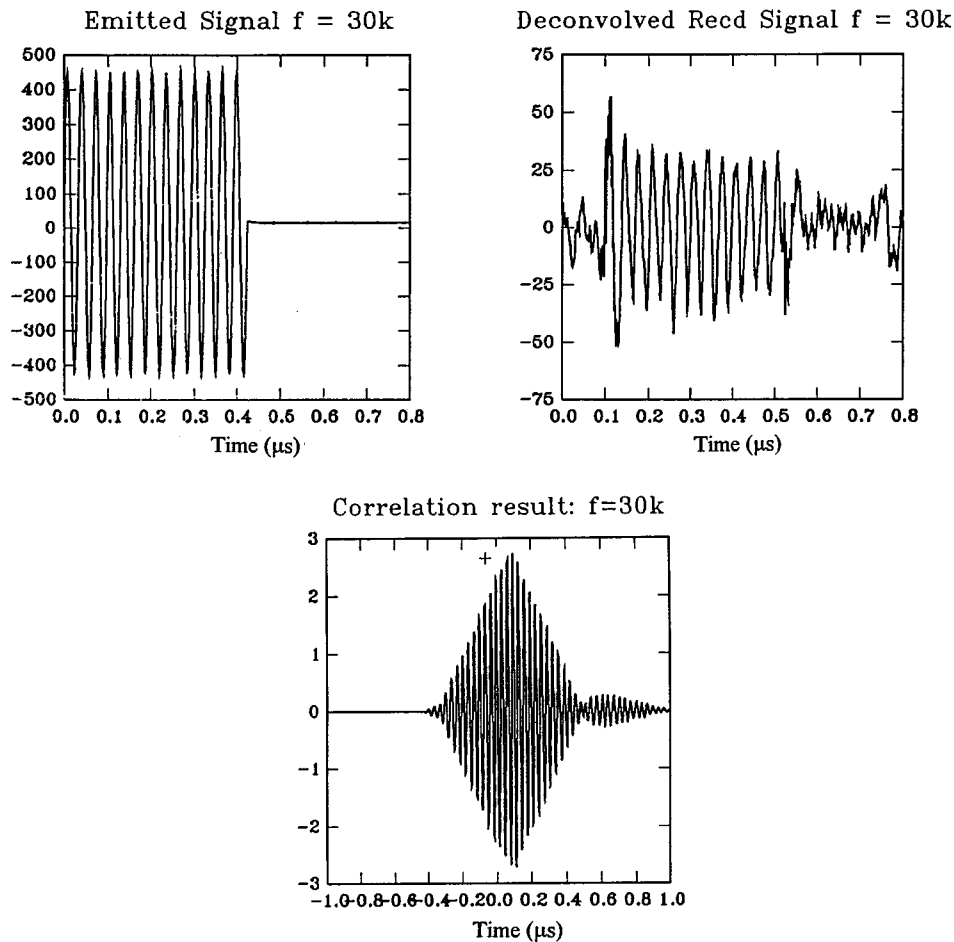


FIG. 11. Example results from cross correlating the emitter excitation signal with the received signal deconvolved with the response of the hydrophone to a square wave. Amplitude scale is arbitrary.

a bubbly medium and receiving the signal with a second hydrophone. The emitted and received signals are acquired and stored. They are then analyzed to obtain the attenuation and sound speed as a function of frequency, and the bubble distribution is deduced. The objective of the experiments is to use these measurements and obtain the sound speed ratio  $u(f)$  and the attenuation  $v(f)$  which form the right-hand sides of Eqs. (9) and (10) in the inverse problem.

In order to achieve the above purpose, we use two hydrophones, an IBM-compatible PC, a data acquisition board, a signal generator, a digital delay generator, and bubble generators. The experiments were performed in a cubic plexi-glass tank of side 1.83 m.

Two model 8103 Brüel & Kjaer hydrophones were used in the experiments. The hydrophones can be operated over a

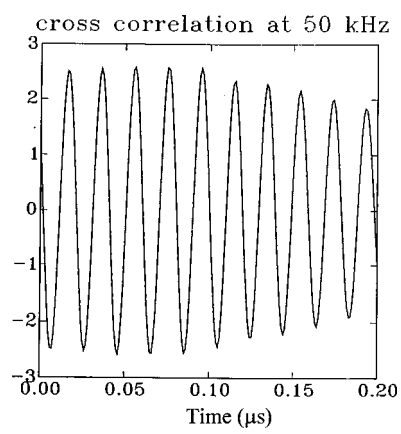


FIG. 12. Example where it is hard to distinguish the highest peak in the result of cross correlating an emitter excitation signal of frequency 50 kHz with the corresponding received response deconvolved with the response of the hydrophone system to a square function. Amplitude scale is arbitrary.

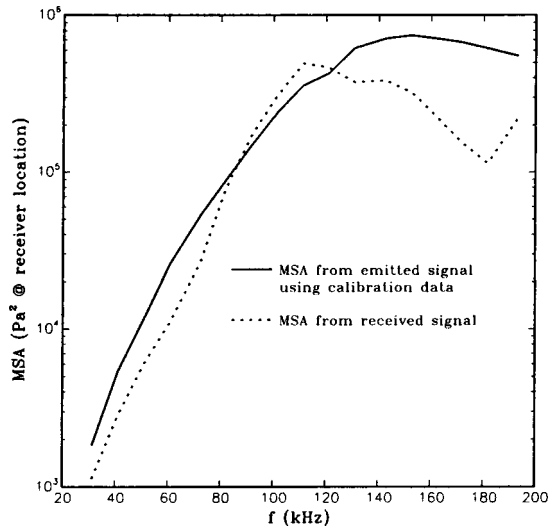


FIG. 13.

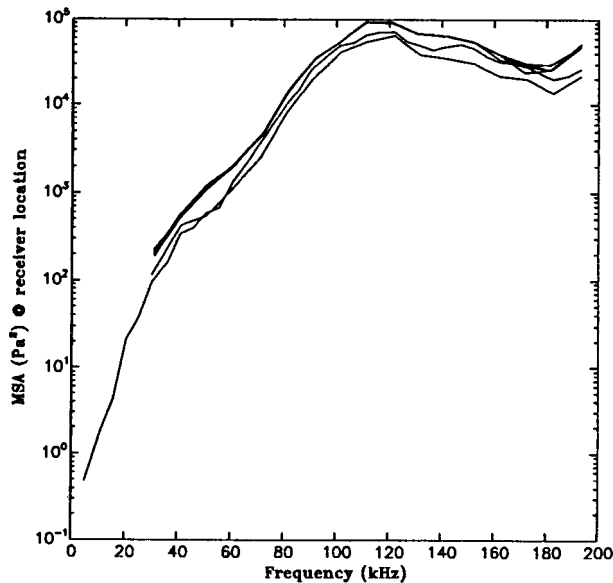


FIG. 14. The MSA power in received signals for experiments performed on different days with no bubbles generated.

range of frequencies from 15 to 190 kHz. The hydrophones are calibrated for sensitivity in both emission and reception, and have a maximum sensitivity at around 120 kHz, which corresponds to their resonant frequency. The frequency of the signal generated was precisely controlled using a voltage-controlled signal generator.

Two types of bubble generators were manufactured and used. Electrolysis at stainless steel wires generated bubbles between 10 and 80  $\mu\text{m}$ . A second technique was based on injecting compressed air through pores in microporous tubes (DYNAPERM®). This produces bubbles of size larger than those generated using electrolysis (10–300  $\mu\text{m}$ ).

The finite size of the tank prohibits the use of continuous signals in the experimental procedure (see Fig. 6). If the duration of emission is too long, reflections from the walls of the tank interfere with the signals emitted, thereby producing composite signals which make data analysis complicated. In order to avoid reflections, the time during which a signal is emitted needs to be shorter than the return time of the first reflected signal. The duration of the emission  $\tau_e$  is given by

$$\tau_e < (d_m - d_{\text{ER}})/c_l, \quad (20)$$

where  $d_m$  is the distance to the closest reflecting boundary. For example, in our experiments  $d_{\text{ER}} = 0.3048$  m,  $d_m = 0.9144$  m, and for  $c_l = 1450$  m/s,  $\tau_e < 0.42$  ms. This requirement imposes a certain amount of low frequency content in the signal. However (as shown by the spectrum of the received signal in Fig. 9 below), this contamination is low. In any case, this defect would be eliminated in the case of measurements in natural waters using this technique, where longer signals could be used.

The signal is received by the other hydrophone and is acquired using the A/D channel 1 of the board. This whole process is repeated successively, thus spanning the interesting range of frequencies (usually 38 values). We experimentally determined that signals generated in one emission die down sufficiently quickly, and that the whole frequency

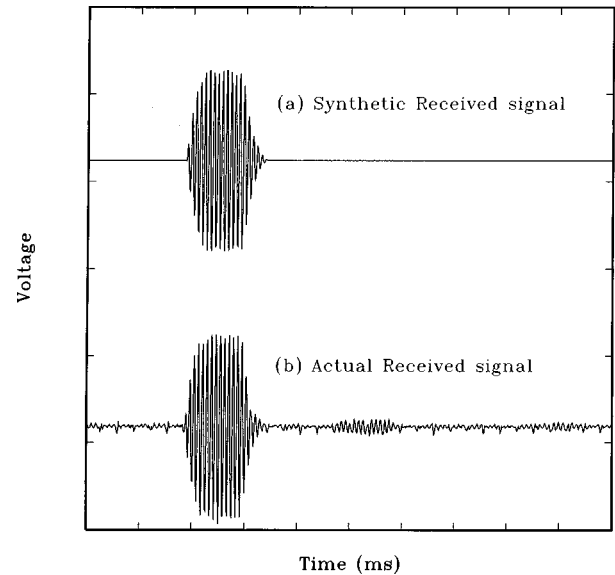


FIG. 15. (a) Synthetically generated received signals assuming a bubble population density and a given emitter frequency. (b) Actual received signal recorded during an experiment for the same conditions and at the same distance.

range could be covered in less than 1 s. Our observations showed that the repeated signals received at any particular frequency changed very little between experiments performed within that interval.

Since the hydrophones have different emitting and receiving sensitivities at different frequencies, an automatic procedure for determining the necessary gain factor for a particular measurement was developed. A preliminary measurement is made at the desired frequencies prior to each experiment, and from the magnitude of the received signal the gain is determined. This procedure was automated and coded, and ensured that the best value of the gain was used for each measurement.

## V. SIGNAL PROCESSING PROCEDURES

Signal processing software was developed to analyze the data acquired and stored during the experiments. The flow chart for the analysis procedure is depicted in Fig. 7.

For each frequency, the received signals are read, and any constant dc components removed using

$$s_i = s'_i - \frac{\sum_{i=1}^N s'_i}{N}. \quad (21)$$

More sophisticated methods for removing the background noise could be incorporated in acoustically noisy environments. Example emitted and received signals for three different frequencies are shown in Fig. 8 with bubbles generated using electrolysis.

A fast Fourier transform (FFT) of the signal is then performed. Example FFT results using emitter excitation and receiver response signals at three typical frequencies (20, 120, and 190 kHz) are shown in Fig. 9 with bubbles being generated. These results show that the received signals are quite pure.

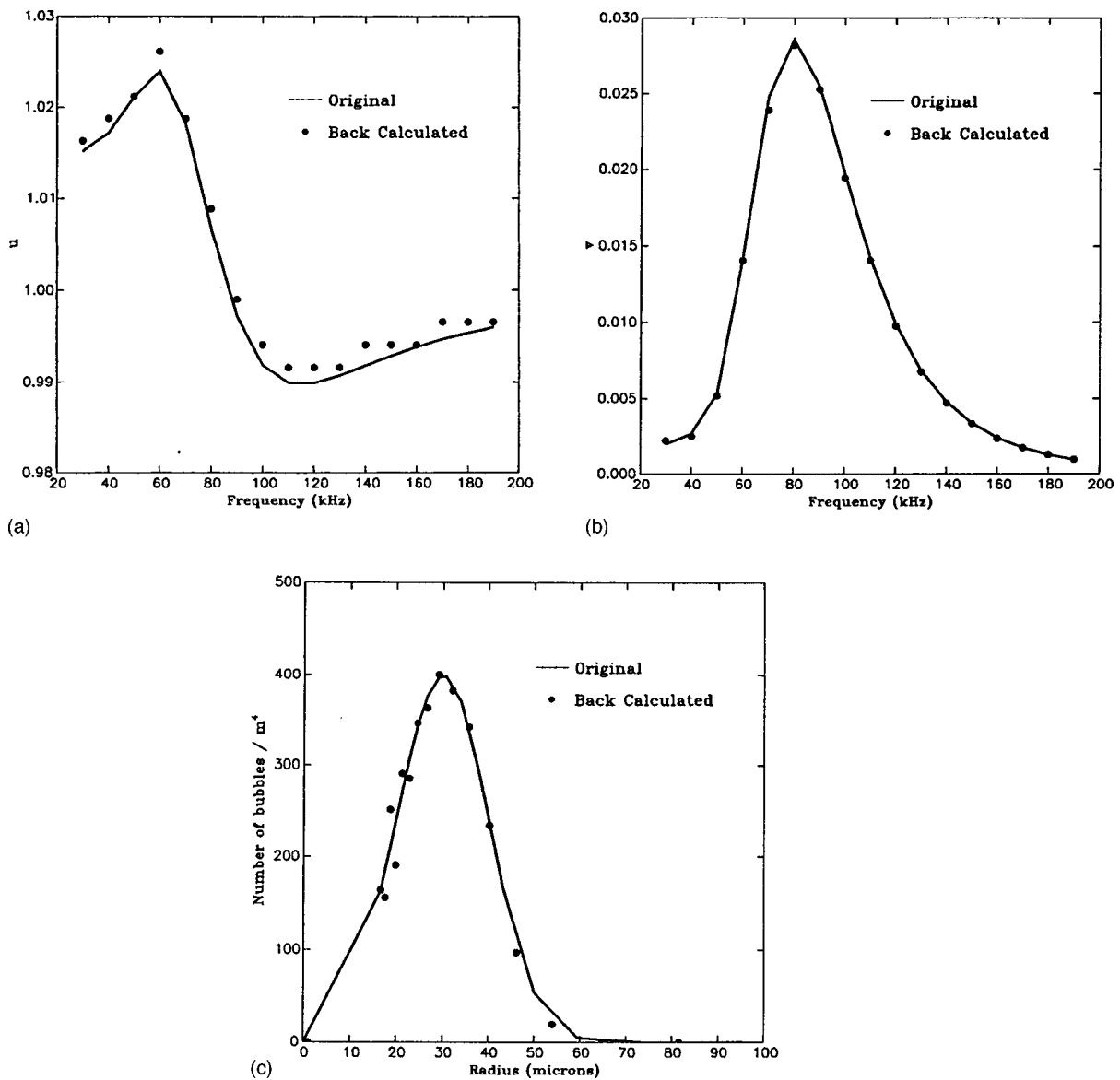


FIG. 16. (a) Original and back-calculated  $u$  curves. (b) Original and back-calculated  $v$  curves. (c) Original and back-calculated bubble distributions.

### A. Processing for phase speed determination

In order to compute the wave speeds a cross correlation is performed between the emitted and received signals. The peak of the cross correlation provides the time,  $\Delta t$ , required for the signal to travel between the emitter and the receiver. The phase speed can then be obtained using the known distance between the emitter and receiver  $d_{ER}$ ,

$$c_m = d_{ER} / \Delta t. \quad (22)$$

Nominally the accuracy of the cross correlation is given by the sampling time, equal to  $1 \mu s$  for our experiments. However, in the presence of real effects such as ringing of the hydrophone or background noise, this estimate may be substantially in error. These errors are removed following the procedure described below.

A sudden change in voltage is rich in high frequencies and leads to a ‘ringing’ of the hydrophone and a finite amount of time to respond. This time affects the results of the cross correlation, and could result in large errors in the

speed of sound calculated unless accounted for. This is done using a deconvolution procedure with the response of the hydrophone to a step function.

Figure 10(a) shows a square wave generated using a function generator that was used to excite the hydrophone. Figure 10(b) shows the signals received by the other hydrophone. The resulting signal after deconvolving the received signal with the response function of the hydrophone is shown in Fig. 10(c). Figure 10(c) shows two impulse functions which are the derivatives of the square wave that was sent. Figure 10(d) shows a blow-up of the initial part of the received signal and is the response of the hydrophone system (emitter and receiver pair) to a step function. The figures illustrate the fact that the hydrophones are not perfect. Figure 10(e) shows the FFT of the response curve and exhibits two dominant frequencies, i.e., around 120 and 240 kHz, which correspond to the resonant frequency of the hydrophone system and the first harmonic.

A typical result of cross-correlating an emitter excitation

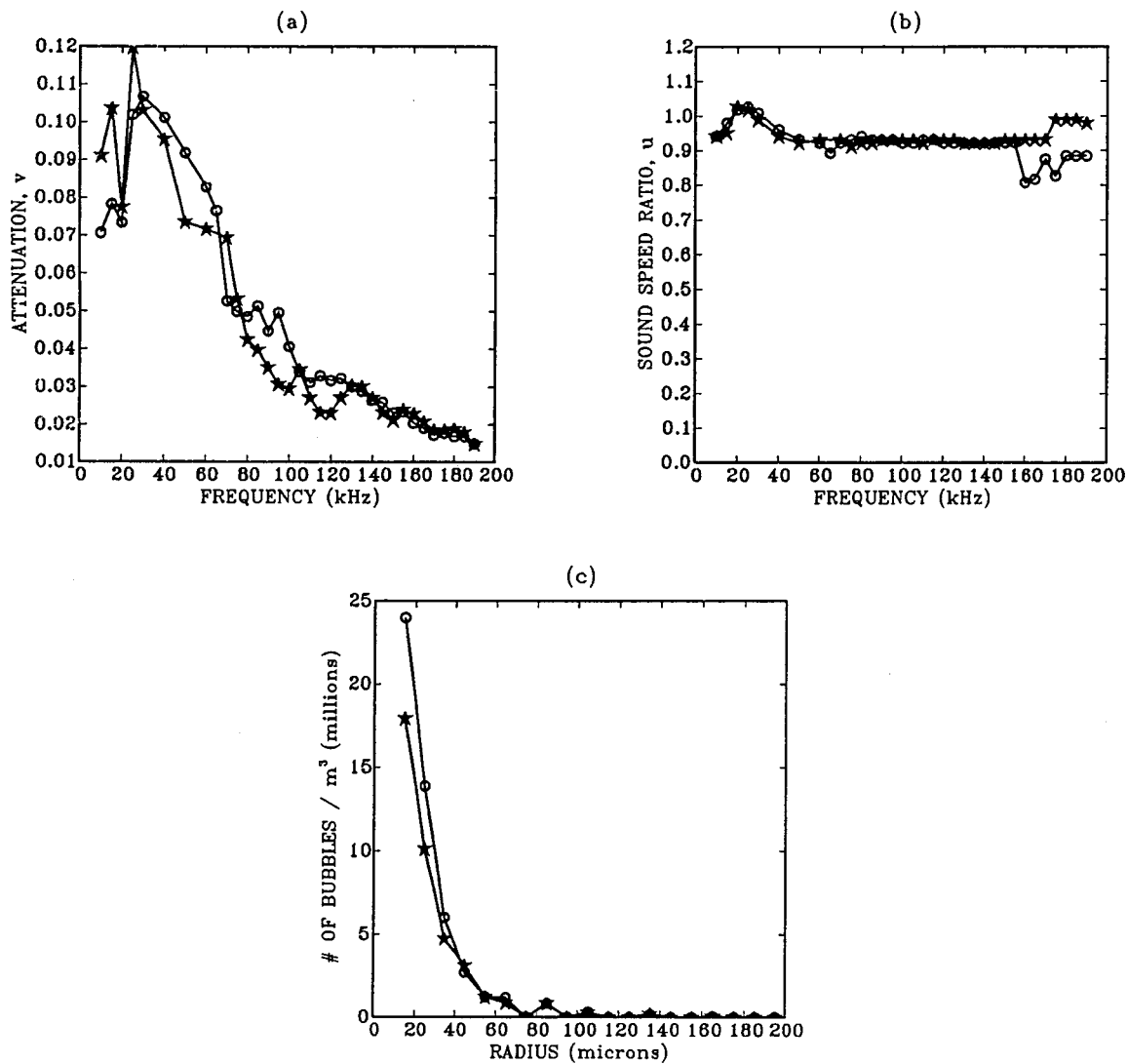


FIG. 17. Results from experiments performed at two different times (2 h apart). (a)  $v$  calculated using emitter sensitivity data and assumption of sphericity to get reference power. (b)  $u$  calculated using deconvolution and curve-fitting. (c) Bubble distribution curves.

and deconvolved received signal pair is shown in Fig. 11.

Figure 12 illustrates that the difference in correlation amplitudes between the highest and second highest peaks could be rather small. If a neighboring peak is chosen, an error of order  $1/f$  will be made in the time estimate. For the smaller frequencies (15 kHz) this *peak uncertainty* can introduce significant errors ( $66 \mu\text{s}$ ), while the possible uncertainty error is lower at higher frequencies ( $5 \mu\text{s}$  at 190 kHz). Considering the very small times and distances involved in the problem, this choice of peaks could result in substantial errors in sound speed evaluation. As a result, the computed/measured curve of sound speed as a function of frequency may not be smooth. To overcome this problem and minimize the probability for error, a condition for smooth curve of sound speed as a function of frequency is used.

The following *a priori* conditions are imposed:

- Values of the speed  $c_m$  obtained using signals that have the lowest signal/noise ratio are given minimum weight.
- Speeds cannot be higher than 1.25 times the speed in pure water.

- Speeds cannot be less than 0.5 times a value based on a low-frequency estimate based on the void fraction.

This procedure enables use of information at all frequencies to select a correct value for the correlation peak at a given frequency, and eliminates the peak uncertainty error.

## B. Processing for $v$

For a given frequency, the mean square amplitude of the pressure wave is estimated using the hydrophone sensitivity calibration data digitized from the charts provided by the manufacturer.

The start and end of emission/reception are determined using the time  $\Delta t$  calculated above. A certain percentage ( $\approx 5\%$ ) of the signal near the start and end is removed to eliminate the influence of the unwanted transients due to the hydrophone response. The remaining portion which has an approximately constant amplitude is used to compute the MSA in the bubbly liquid.

To obtain the quantity  $v$  we need to obtain the MSA under conditions of transmission through pure water. Two

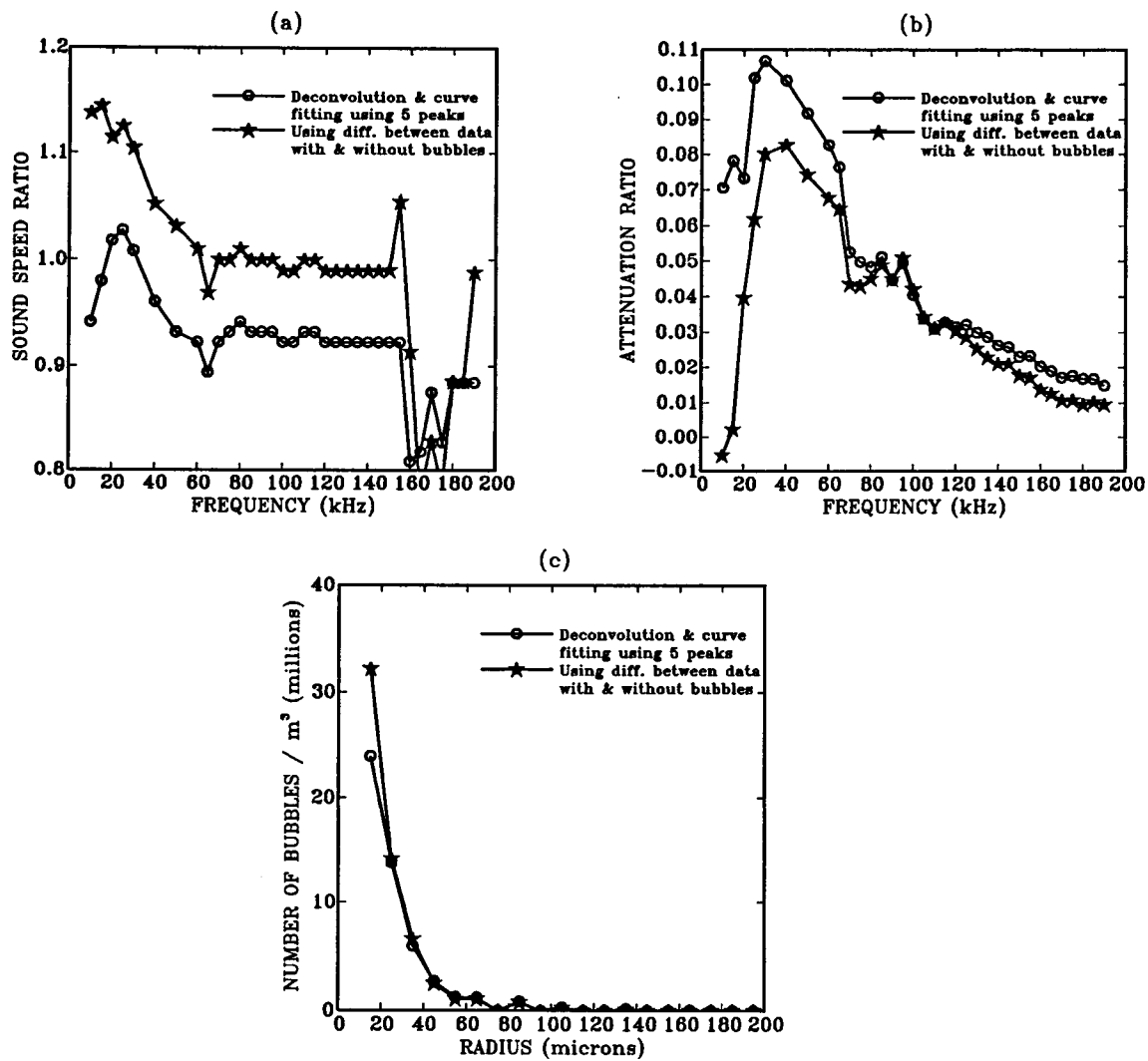


FIG. 18. Comparison of results analyzed using two different methods to get  $u$  and  $v$  curves: a deconvolution method, and comparison with no injected bubble test.

methods to obtain the reference MSA were used.

In the first method, using the manufacturer's calibration for the hydrophone along with the assumption that the waves are emitted spherically enabled calculation of the reference MSA. This method was tested by performing experiments in the tank with no bubbles being generated. The comparison of the expected and measured MSA is shown in Fig. 13. While the two curves are relatively close, the difference in the quantity could result in substantial amounts of spurious bubbles being predicted.

In the second technique a calibration phase of the experiments is performed in "pure" water (i.e., with no bubbles being injected). The reference MSA is calculated using the recorded received signal data. This approach has the advantage of eliminating sources of error that are common to the two measurements. Experiments with no bubbles generated were performed on different days and the MSA of the different received signals computed as a function of frequency is shown in Fig. 14. The fact that the different experiments without bubbles are repeatable indicates that the already existing bubble nuclei population in the tank water is very stable. Based on the repeatability of these experiments

we decided to use a comparison method for the calculation of the attenuation factor  $v$ . It was felt that such a procedure would not cause a large error in the measurements when bubble populations were being generated, as the microscopic population already in the tank was likely to be much smaller than the bubble population being generated, and have negligible influence on the attenuation and phase velocities at the frequencies considered.

### C. Verification of solution procedure with synthetic data

The various steps used to extract the  $u$  and  $v$  data from the various digitized signals and the possible errors introduced could have a bearing on the inverse problem accuracy. We thus performed using synthetic data an end-to-end checkout of the developed algorithms for consistency. The synthetic data were generated by assuming a bubble distribution (shown earlier in Fig. 2). Then the various numerical steps were calculated as follows.

- (1)  $u$  and  $v$  were obtained as functions of frequency by solving the forward problem.

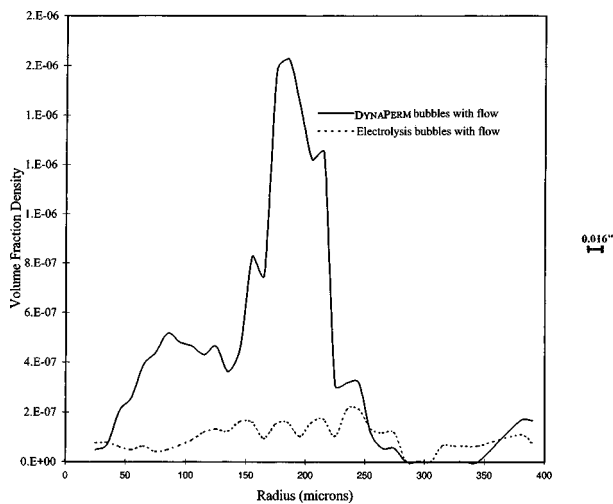


FIG. 19. The volume fraction density of bubbles at a given radius versus the radius of bubbles is shown for the electrolysis and porous tube bubblers with flow. The density was computed by integrating the bubble density function over bins of size  $10 \mu\text{m}$ .

- (2) The excitation signal was convolved with the response of the hydrophone system to a step function.
- (3) The resulting convolved voltage signal was converted to pressure using the emitter sensitivity curve at the given frequency.
- (4) Using  $u$ , the time elapsed  $\Delta T$  between the emitter excitation and synthetic receiver response signals was obtained.
- (5) The attenuation due to the bubbles was obtained using the  $v$  value at the given frequency.
- (6) The emitter excitation signals and the synthetically generated received signals were used by the signal analysis program to yield back  $u$  and  $v$  curves as functions of frequency. These  $u$  and  $v$  curves are used by the inverse problem program to obtain back the desired bubble distribution curve.

Figure 15 compares a synthetically generated received signal with a frequency of 120 kHz for the emission with an actual received signal recorded during an experiment. The figure clearly illustrates the closeness of the synthetically generated received signals to the actual received signals. Figure 16(a) and (b) compare the  $u$  and  $v$  curves obtained after performing signal analysis using the synthetic data with the corresponding original curves that were used to generate the data. Figure 16(c) compares the back calculated bubble distributions with the original assumed distributions.

These figures show that the back calculated  $u$  curve follows the original  $u$  curve. The small discrepancy between the two can be related to the inaccuracy resulting from the limited sampling frequency of the data acquisition board which results in a margin of error on  $u$  of  $\pm 0.005$ . For the particular experimental setup,  $u$  is better estimated at large distances between the emitting and receiving hydrophones. However, the larger the distance, the greater is the attenuation and the smaller the amplitude of the signals. The resolution in  $v$  decreases with decrease in amplitude of the signal if the voltage gain factor of the data acquisition board is kept unchanged. As discussed before, the distance between the hy-

drophones is also limited by the finite size of the tank and the reflections which could combine with the direct signal.

## VI. BUBBLE SIZE MEASUREMENT EXPERIMENTS

The two hydrophones were placed at the same vertical level at the center of the tank, with a separation distance between them of 0.152 m. In order to minimize noise, the same emission frequency was repeated many times, the signals were stored, and an average generated. Experiments were first performed with no artificial bubbles injection.

Bubbles were generated using electrolysis on stainless steel wires of diameter 0.4 mm. Figure 17 shows typical analysis results corresponding to data obtained in this case. The duration of emission of the sinusoidal signals was chosen to be 0.4 ms based on Eq. (20). Figure 17(a) shows the  $v$  curves computed at two different times about 2 h apart and Fig. 17(b) shows the corresponding  $u$  curves. The  $v$  data were computed using the calibration curves and the  $u$  data were computed using the combination of deconvolution and curve fitting procedures described earlier. Figure 17(c) shows the corresponding bubble distribution curves. The bubble distribution curves from the inverse problem were grouped by dividing the guesses for minimum and maximum radii  $a_{lo}$  and  $a_{hi}$  into 100 bins. In this case the size of a bin was about  $10 \mu\text{m}$ . It can be seen from the figures that the data are repeatable, but that the experimental and analysis procedure limits the measurements to bubble sizes larger than  $15 \mu\text{m}$ . This can be improved with better instrumentation.

Figure 18(a) and (b) compares the  $u$  and  $v$  curves obtained using two different methods. The solid lines with circles show results obtained using a method similar to that of Fig. 17. The lines with stars represent results obtained by using the difference between data with and without bubbles to compute  $u$  and  $v$  as described earlier. The bubble size distributions obtained in each case are shown in Fig. 18(c), and appear to be very close except at the low bubble radii where the experimental errors are the largest.

## VII. VALIDATION OF RESULTS

Some of the results obtained using the acoustic technique were attempted to be validated using microphotography. Results are presented here for one case using the electrolysis bubble generator and one case using the DYNAPERM bubble generator. Figure 19 shows the void fraction distribution corresponding to these two types of generators.

The image processing technique we used to obtain the bubble population from the photographs is as follows: A photograph of the generated bubbles with a reference scale was taken while the experiments were performed. The photograph was then scanned at 150 dots per inch (dpi). A threshold level for the gray-scale image was determined based on the closeness of comparison between the thresholded image and the gray-scale image. The width and height in pixels, the dpi, and the threshold level for the image were noted. From the resulting raw image the area in pixels for each bubble detected was obtained using developed image processing software, and converted to an equivalent radius. The resulting radii were then grouped into a number of bins

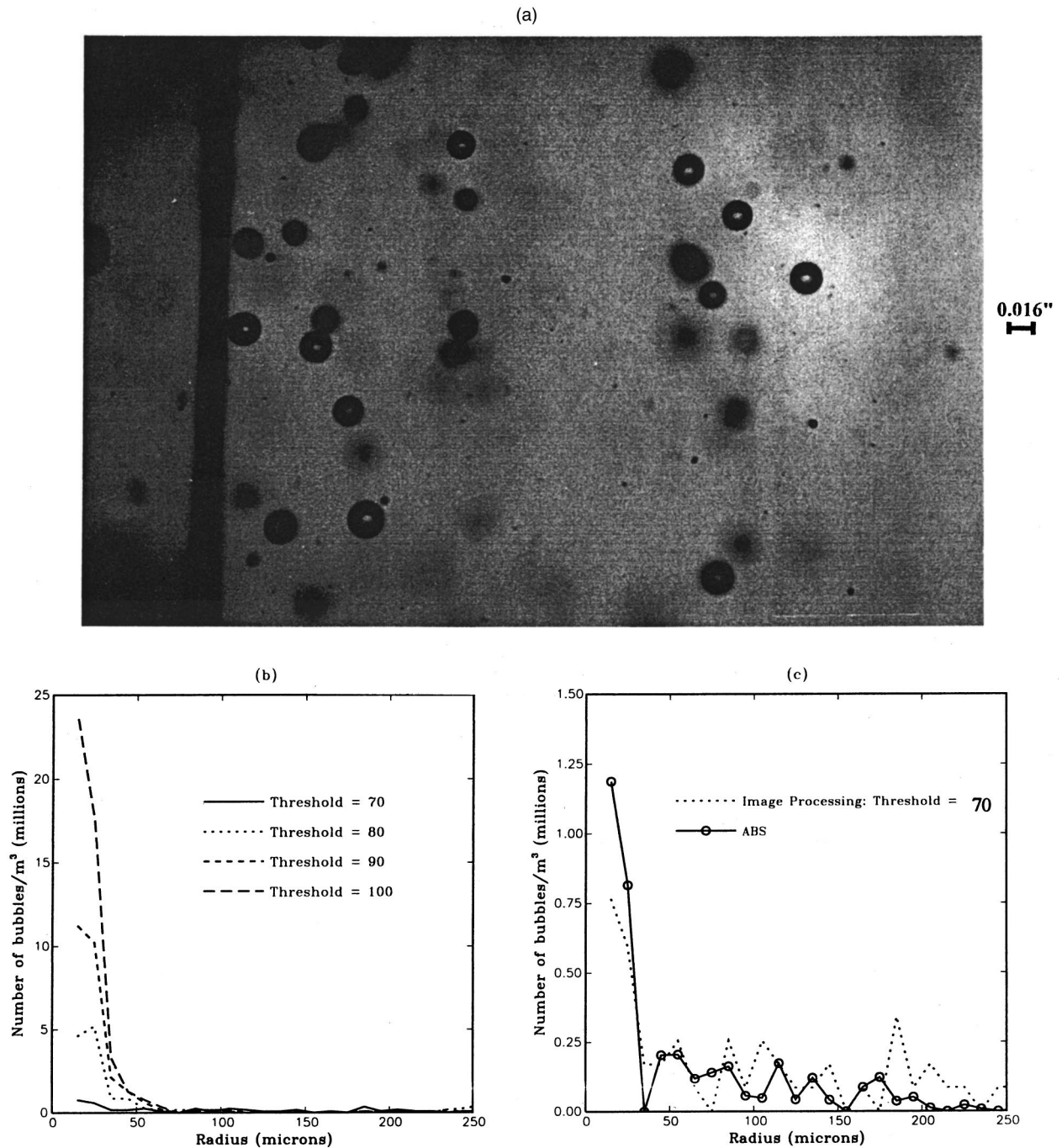


FIG. 20. (a) Example photograph of bubbles generated using the DYNAPERM tubes with no shear flow. (b) Results of analyzing the photo using image processing software with threshold levels of 70, 80, 90, and 100. (c) Comparison of bubble distribution from photography with that from the present procedure.

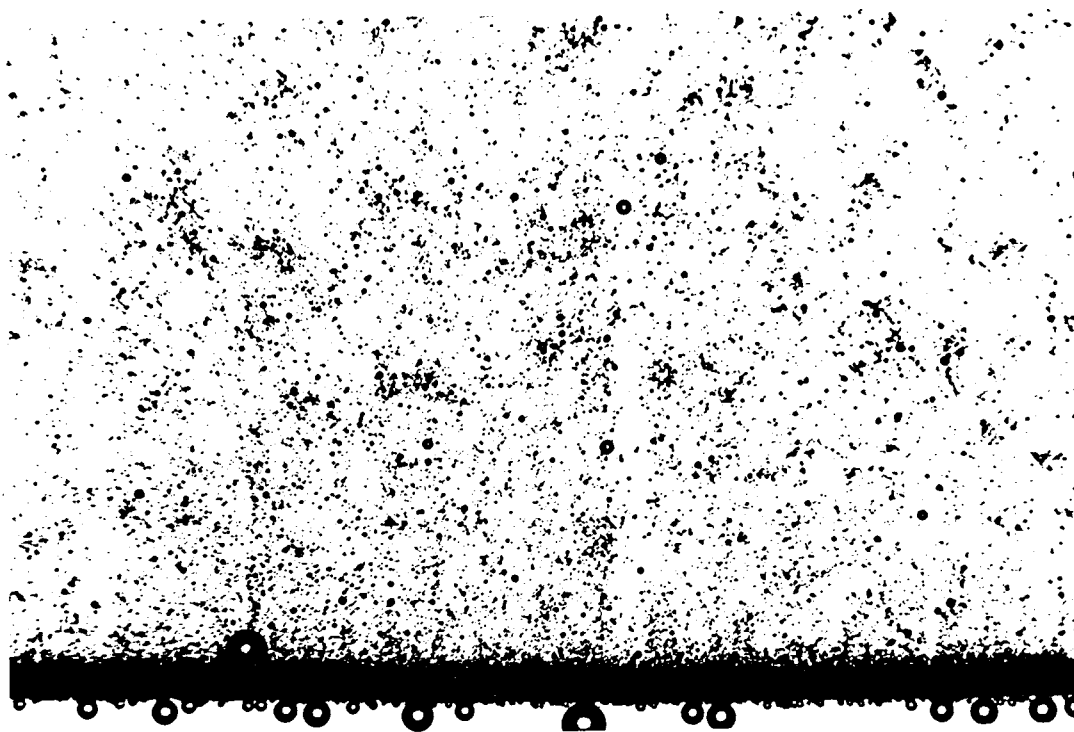
obtained by subdividing the range spanned between the maximum and minimum radius of the bubbles, and using the area of the scanned image were converted to numbers per square meter. The data was extrapolated to numbers per cubic meter by using the depth of field of the photograph.

Figure 20(a) shows an example photograph taken of the bubbles generated using DYNAPERM tubes without shear flow. Figure 20(b) shows the result of image analysis of the photograph using different threshold levels and a depth of field of 7.5 cm. As can be seen from the figure, the number of bubbles detected is very sensitive to the threshold level selected. However, the shape of the bubble distribution curve

remains the same. A threshold level of 70 was selected on the basis that it yielded a binary image that compared best with the original grayscale image.

Figure 20(c) compares the bubble distribution curve obtained from processing the photograph at a threshold level of 70 with that from the present solution. The figure illustrates a reasonable comparison between the two methods. One drawback of the photograph shown is that it sampled a very small area ( $\approx 2 \text{ cm}^2$ ) relative to the size of the bubbles involved and as a result is prone to substantial variance in the bubble population estimates.

Figures 21(a) shows an example photograph taken dur-



(a)

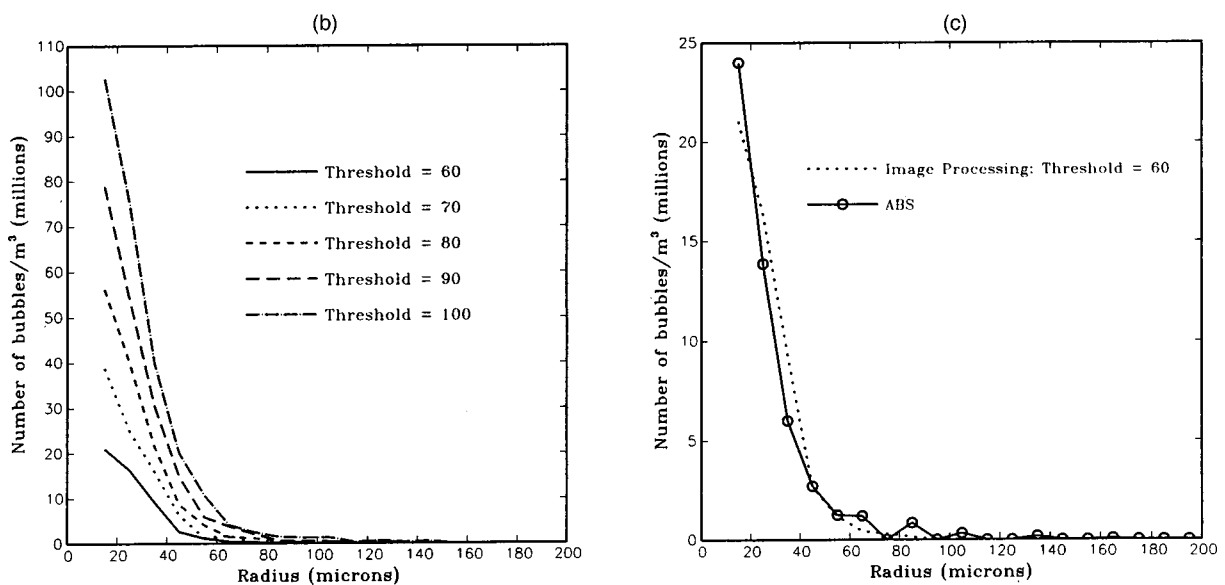


FIG. 21. (a) Example photograph of bubbles generated with the electrolysis bubbler. (b) Results of analyzing the photo using image processing software with threshold levels of 60, 70, 80, 90, and 100. (c) Comparison of bubble distribution from photography with that from the present procedure.

ing experiments performed with bubbles being generated using electrolysis. Figure 21(b) shows the result of analyzing the photo using different threshold levels to convert the gray scale to a binary image. A threshold level of 60 was selected on the basis that it yielded a binary image that compared best with the original gray scale image. Figure 21(c) compares the bubble distribution curve obtained from processing the photograph at a threshold level of 60 with that from the present solution. The figure illustrates again a very good comparison between the two techniques.

Because of the subjectivity in the choice of the threshold, these results only validate the fact that the shapes of the bubble populations are similar. Because of the difficulties

associated with different methods, the absolute validation of any technique for measuring microscopic bubbles remains an unsolved experimental problem.

## VIII. SUMMARY AND CONCLUSIONS

The dispersion relation for propagation of monochromatic waves in bubbly liquids was used to obtain two equations for the bubble population density. These equations,

which are ill posed, were regularized by imposing different constraints on the solutions, including the fact that the equations must be satisfied simultaneously, that the bubble number density has to be positive, and that the volume fraction is bounded. A constrained minimization procedure based on the simplex method was used to solve these equations.

The accuracy of the solution for different problem discretizations was studied and a discretization that resulted in uniform accuracy of the solution for different test problems developed. The effect of choices of different objective functions and constraints was also studied. Based on these results a procedure for the solution of the ill-posed equations of bubble counting was developed. This procedure was compared with conventional formulas for estimating bubble and was found to be much more accurate. While the developed procedure for the solution of the inverse problem is more intensive computationally than the conventional formula, the algorithms we have developed are efficient and can achieve solution relatively quickly.

Experimental procedures were developed to measure the phase velocity and attenuation simultaneously for monochromatic acoustic waves in bubbly liquids. A signal analysis procedure was developed that enabled deduction of these quantities from the measurements, and that accounted for the effect of the ringing of the transducers by using deconvolution. The analysis procedure was also verified on synthetic signals.

Several experiments were performed with artificially generated bubbles, and the resulting bubble populations obtained. For some of the experiments simultaneous microphotography was performed. A procedure to obtain bubble size distributions from the photographs was also developed. Comparisons of the populations indicate that the bubble size distribution obtained by the two techniques are similar.

In ongoing work, the developed method is being packaged into a user friendly Windows-based application that integrates the different components of the system, and produces near real-time estimates of bubble distributions. Efforts are underway to produce instrumentation for bubble detection, void-fraction measurement, and bubble population measurement using the developed techniques. This instrument—the *Acoustic Bubble Spectrometer*—is being commercialized.

## ACKNOWLEDGMENTS

This work was supported by the National Science Foundation under Grant Nos. III-9160484 and III-9301379. We would like to thank the associate editor and an anonymous referee for several suggestions for improvement of the manuscript.

<sup>1</sup>H. Medwin, "In situ acoustic measurements of bubble populations in coastal ocean waters," *J. Geophys. Res.* **75**, 599–611 (1970).

<sup>2</sup>H. Medwin, "Counting bubbles acoustically: a review," *Ultrasonics* **15**, 7–13 (1977).

<sup>3</sup>H. Medwin, "Acoustical determination of bubble-size spectra," *J. Acoust. Soc. Am.* **62**, 1041–1044 (1977).

<sup>4</sup>N. Breitz and H. Medwin, "Instrumentation for *in situ* acoustical measurements of bubble spectra under breaking waves," *J. Acoust. Soc. Am.* **86**, 739–743 (1989).

<sup>5</sup>H. Medwin and N. D. Breitz, "Ambient and transient bubble spectral densities in quiescent seas and under spilling breakers," *J. Geophys. Res.* **94**, 12 751–12 759 (1989).

<sup>6</sup>A. Lovik, "Acoustic Measurements of the Gas Bubble Spectrum in Water," in *Cavitation and Inhomogeneities in Underwater Acoustics*, edited by W. Lauterborn (Springer-Verlag, Berlin, 1980), pp. 211–218.

<sup>7</sup>I. P. Schippers, "Density of Air-Bubbles Below the Sea Surface, Theory and Experiments," in *Cavitation and Inhomogeneities in Underwater Acoustics*, edited by W. Lauterborn (Springer-Verlag, Berlin, 1980), pp. 205–210.

<sup>8</sup>P. A. Crowther, "Acoustical Scattering from near-surface bubble layers," in *Cavitation and Inhomogeneities in Underwater Acoustics*, edited by W. Lauterborn (Springer-Verlag, Berlin, 1980), pp. 187–193.

<sup>9</sup>T. J. O'Hearn, "Cavitation inception scale effects," Ph.D. thesis, California Institute of Technology, 1987.

<sup>10</sup>S. Prabhukumar, R. Duraiswami, and G. L. Chahine, "Bubble size measurement using inverse acoustic scattering: Theory & Experiments," *ASME Cavitation & Multiphase Flow Forum*, 1996.

<sup>11</sup>S. Vagle and D. M. Farmer, "The measurement of Bubble-Size Distributions by Acoustical Backscatter," *J. Atmos. Ocean. Technol.* **9**, 630–644 (1992).

<sup>12</sup>T. Ohern, J. Torczynski, S. Tassin, S. Ceccio, G. Chahine, R. Duraiswami, and K. Sarkar, "Development of an Electrical Impedance Tomography System for an Air-Water Vertical Bubble Column," *Proceedings, Forum on Measurement Techniques in Multiphase Flows, ASME IMEC&E* (1995).

<sup>13</sup>D. M. Oldenzel, "A new instrument in cavitation research: the cavitation susceptibility meter," *J. Fluids Eng.* **104**, 136–142 (1982).

<sup>14</sup>F. MacIntyre, "On reconciling optical and acoustical bubble spectra in the mixed layer," in *Oceanic Whitecaps*, edited by E. C. Monahan and G. Macniocaill (Reidel, New York, 1986), pp. 75–94.

<sup>15</sup>R. Wildt, editor, *Physics of Sound in the Sea, Part IV* (National Research Council, Dept. of Defense, Washington, DC, 1949).

<sup>16</sup>R. E. Caffisch, M. J. Miksis, G. C. Papanicolau, and L. Ting, "Effective Equations for wave propagation in bubbly liquids," *J. Fluid Mech.* **153**, 259–273 (1985).

<sup>17</sup>K. W. Commander and A. Prosperetti, "Linear pressure waves in bubbly liquids: Comparison between theory and experiments," *J. Acoust. Soc. Am.* **85**, 732–746 (1989).

<sup>18</sup>R. Duraiswami and G. L. Chahine, "Bubble density measurement using an inverse acoustic scattering technique," NSF SBIR Phase I project report, also Dynaflow Technical Report 92004-1 (1992).

<sup>19</sup>R. Duraiswami, "Bubble Density Measurement Using an Inverse Acoustic Scattering Technique," *ASME Cavitation and Multiphase Flow Forum*, Washington, DC, June 1993, edited by O. Furuya (ASME, New York, 1993), FED Vol. 153, pp. 67–74.

<sup>20</sup>A. Prosperetti, "Physics of Acoustic Cavitation," in *Frontiers in Physical Acoustics XCIII Corso*, (Soc. Italiana di Fisica, Bologna, Italy, 1986), pp. 145–188.

<sup>21</sup>K. Sarkar and A. Prosperetti, "Coherent and incoherent scattering by oceanic bubbles," *J. Acoust. Soc. Am.* **96**, 332–341 (1994).

<sup>22</sup>R. Kress, *Linear Integral Equations* (Springer-Verlag, Berlin, 1989), particularly Chaps. 15–17.

<sup>23</sup>S. W. Provencher and R. H. Vogel, "Regularization techniques for inverse problems in molecular biology," in *Numerical Treatment of Inverse Problems in Differential and Integral Equations*, edited by P. Deuffhard and E. Hairer (Birkhauser, Boston, 1983).

<sup>24</sup>K. W. Commander and R. J. McDonald, "Finite-element solution of the inverse problem in bubble swarm acoustics," *J. Acoust. Soc. Am.* **89**, 592–597 (1991).

<sup>25</sup>I. Barrodale and F. D. K. Roberts, "Solution of an overdetermined system of equations in the  $l_1$  norm," *Commun. ACM* **17**, 319–320 (1974).

<sup>26</sup>K. W. Commander and E. Moritz, "Off resonance contributions to acoustical bubble spectra," *J. Acoust. Soc. Am.* **89**, 592–597 (1989).